

Synthesis and Enhanced Field-Emission of Thin-Walled, Open-Ended, and Well-Aligned N-Doped Carbon Nanotubes

Tongxiang Cui · Ruitao Lv · Feiyu Kang ·

Qiang Hu · Jialin Gu · Kunlin Wang ·

Dehai Wu

Received: 10 January 2010/Accepted: 16 March 2010/Published online: 31 March 2010
© The Author(s) 2010. This article is published with open access at Springerlink.com

Abstract Thin-walled, open-ended, and well-aligned N-doped carbon nanotubes (CNTs) on the quartz slides were synthesized by using acetonitrile as carbon sources. As-obtained products possess large thin-walled index (TWI, defined as the ratio of inner diameter and wall thickness of a CNT). The effect of temperature on the growth of CNTs using acetonitrile as the carbon source was also investigated. It is found that the diameter, the TWI of CNTs increase and the Fe encapsulation in CNTs decreases as the growth temperature rises in the range of 780–860°C. When the growth temperature is kept at 860°C, CNTs with TWI = 6.2 can be obtained. It was found that the field-emission properties became better as CNT growth temperatures increased from 780 to 860°C. The lowest turn-on and threshold field was 0.27 and 0.49 V/μm, respectively. And the best field-enhancement factors reached 1.09×10^5 , which is significantly improved about an order of magnitude compared with previous reports. In this study, about $30 \times 50 \text{ mm}^2$ free-standing film of thin-walled open-ended well-aligned N-doped carbon nanotubes was

also prepared. The free-standing film can be transferred easily to other substrates, which would promote their applications in different fields.

Keywords Carbon nanotubes · Thin-walled open-ended and aligned · Thin-walled index · Bamboo-shaped carbon nanotubes · Field emission · Free-standing

Introduction

Since the discovery in 1991 [1], carbon nanotubes (CNTs) have attracted much attention due to their unique electronic and mechanical properties [2]. Numerous articles have reported studies on their field-emission properties [3–8]. Previous study of our group had shown that thin-walled CNTs possessed better field-emission properties than thick-walled ones [5]. Quantitative analysis and experiment showed that open-ended CNTs had better field-emission properties than closed-ended ones [8, 9], and it was also found that aligned CNTs had better field-emission properties than random ones [7]. Nowadays, the synthesis of N-doped CNTs has attracted considerable attention. There were many articles reported on the synthesis and properties of N-doped CNTs [10–13]. It was found that doping nitrogen into CNTs could improve their field-emission properties [14, 15]. Thus, thin-walled open-ended well-aligned N-doped CNTs are expected to have excellent field-emission properties; however, there are few reports on the synthesis of this kind of CNTs. In this study, floating catalyst CVD method was used to synthesize thin-walled open-ended N-doped CNT arrays by using acetonitrile as the carbon source. As-obtained products are multi-walled CNTs and have a large thin-walled index [16] (TWI, defined as the ratio of inner diameter and wall thickness of

T. Cui · R. Lv · F. Kang (✉) · J. Gu
Laboratory of Advanced Materials, Department of Materials
Science and Engineering, Tsinghua University,
Beijing 100084, China
e-mail: fykang@tsinghua.edu.cn

Q. Hu
Department of Electronic Engineering, Tsinghua University,
Beijing 100084, China

K. Wang · D. Wu
Department of Mechanical Engineering, Key Laboratory
for Advanced Manufacturing by Materials Processing
Technology of Ministry of Education, Tsinghua University,
Beijing 100084, China

a CNT). Furthermore, enhanced field-emission properties were also demonstrated in this study.

The synthesis of vertically aligned CNT arrays was investigated by many researchers [3, 4, 6, 14, 17, 18]; however, it is still a challenge to obtain free-standing membranes of CNTs without destroying their aligned structure. The fabrication of flexible free-standing CNT membranes has been reported by many publications [18–27]. The applications of the free-standing membranes are in diverse fields, such as lithium ion batteries [21, 25], electromechanical actuators [22], electron-emitting cathodes [23], sensor devices [24], hydrogen fuel cells [26], and so on. Up to now, the most frequently used method for the fabrication of free-standing membranes is transferring CNTs onto plastic substrates by photolithograph or spin-coating methods [18, 21], and filtration of CNT suspension [25]. However, these methods are somehow limited due to the expensive experimental set-up and/or complex processes. In this study, a simple method was proposed to obtain free-standing membranes of as-synthesized N-doped CNTs, which might be helpful to their applications in many fields.

Experimental

The experimental setup and procedure are similar to that described in our previous report about Fe-filled CNTs [28], but we use acetonitrile rather than chlorine-containing benzene as carbon source. Ferrocene powders were dissolved in acetonitrile to form solutions with concentration of 20 mg/ml, and fed into CVD furnace by a syringe pump at a constant rate of 0.4 ml/min for 30 min. A mixture of Ar and H₂ was flowing through the system at 2,000 and 300 sccm, respectively. A quartz slide was put into the middle of furnace to collect CNTs at a reaction temperature. In our previous study, we found the suitable reaction temperature for aligned carbon nanotube was 800–840°C using xylene as the carbon source [29]. The reaction temperature in present case is thus set in the range of 780–860°C for investigation.

The scanning electron microscope (SEM) images were obtained by a JOEL JSM-6460 LV SEM. The transmission electron microscope (TEM) images were taken by a TEM with a model of JEM-200 CX, using an accelerating voltage of 200 kV. Thermogravimetric analysis (TGA) results were obtained by measuring 6 mg samples in air flow at a heating rate of 20°C/min. The X-ray photoelectron spectroscopy (XPS) spectra were obtained by PHI Quantera. The XPS measurements were carried out in a vacuum chamber of 1.4×10^{-8} Torr, using Al K_α (1486.7 eV) laser excitation. Raman spectra were performed on microscopic confocal Raman spectrometer (Renishaw RM

2000) using 632.8 nm (1.96 eV) laser excitation. The field-emission measurements were carried out in a vacuum chamber of 2.2×10^{-6} Torr with CNT samples on silicon wafer as cathode. A glass plate with transparent indium tin oxide (ITO) electrode and phosphor was used as both an anode to collect electrons and a display screen. Distance between anode and top of CNT samples was kept at 2.0 mm.

Results and Discussion

Figure 1 shows the SEM images of as-grown products with different temperatures. It can be seen from Fig. 1a–c that the products are all well-aligned at different growth temperatures. The lengths of the CNTs are 46.6, 44.3, and 47.5 μm for 780, 820, and 860°C, respectively. It can be seen that the surfaces of as-grown products are very clean and free from impurity particles. As seen from Fig. 1d, the CNTs grown at 860°C are open-ended, in fact the CNTs are all open-ended in the range of 780–860°C. This is of vital importance for their field-emission properties.

Figure 2 shows the TEM images of samples produced at different temperatures. Figure 2a–c are typical TEM images of CNTs prepared at 780, 820, and 860°C, respectively. It can be seen from Fig. 2a–c that all these products possess large TWI. The products are open-ended, which is in agreement with the SEM observations. The typical tip structure of as-obtained product is shown in Fig. 2d, and the CNT is multi-walled CNT as shown in Fig. 2e. TEM observations also reveal that the CNTs have bamboo-shaped structures, which are similar to many reports about N-doped CNTs [11, 13, 30, 31]. Bamboo-shaped CNTs are usually formed because of the formation of 5-member ring structures [32]. In present case, the formation of bamboo-shaped CNTs is more possibly attributed to the doping of nitrogen into CNTs because of the easy tendency of 5-member ring structure formation.

It can be seen from Fig. 2a–c that the diameter and TWI become larger as temperature rises. The effect of temperature on diameter in present study is similar to that reported by Yadav, et al. [30], but no obvious temperature effect on TWI was shown in their case. In present study, a possible explanation for temperature effect on TWI is that larger-sized catalyst particles lead to wider inner cavity of the CNTs, and therefore larger TWI is obtained.

The TGA results of the as-grown products at different temperatures (Fig. 3) show that the Fe encapsulation in CNTs decreases as temperature rises. No remarkable weight loss or gain occurs before 450°C in air, which demonstrates that as-grown products possess high thermal stability (see A → B part of Fig. 3). When all the CNTs and Fe metals are fully oxidized, the sample weight will

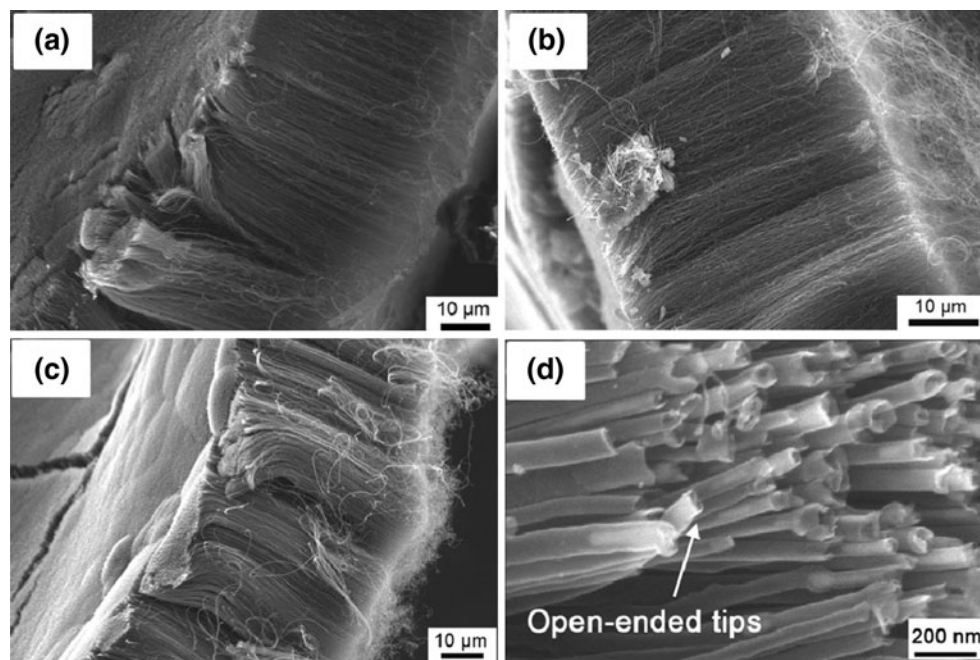


Fig. 1 SEM images of as-grown products at different growth temperatures: **a** 780°C sample, **b** 820°C sample, **c** 860°C sample, **d** Open-ended tips of the 860°C CNT sample

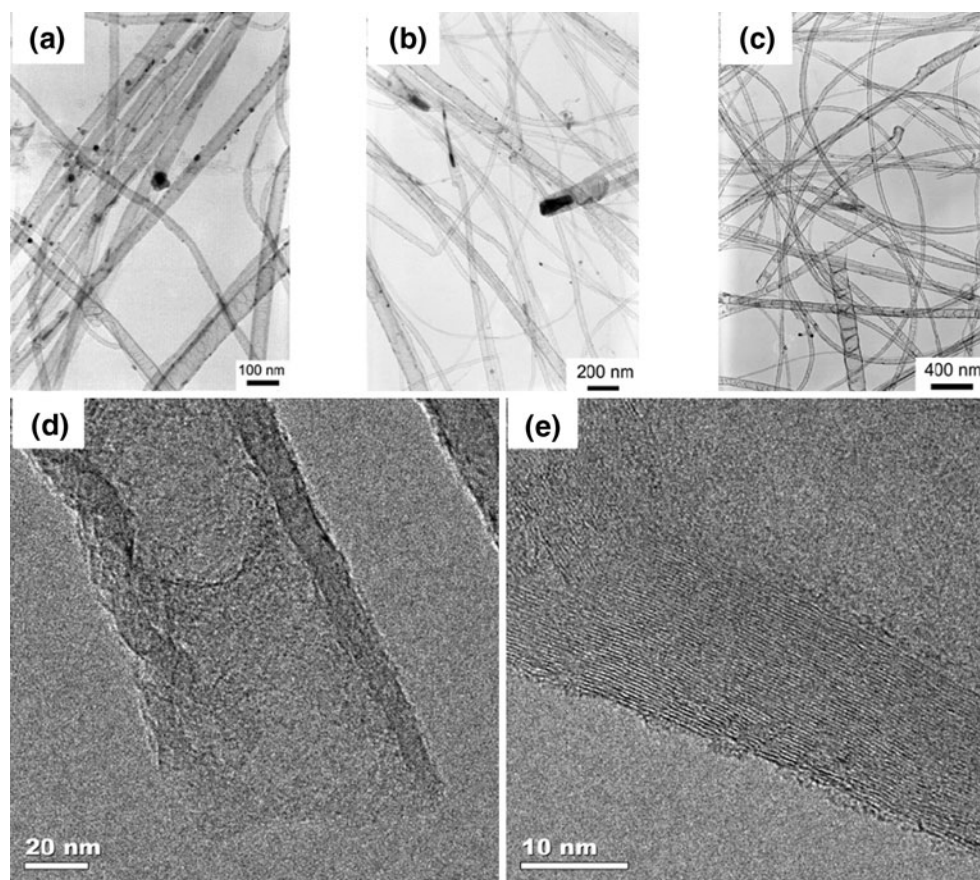


Fig. 2 TEM images of the as-grown products at different growth temperature: **a–c** are the low-magnification TEM images of a 780, 820, and 860°C sample; **d, e** are the high-magnification TEM images of a 860°C sample

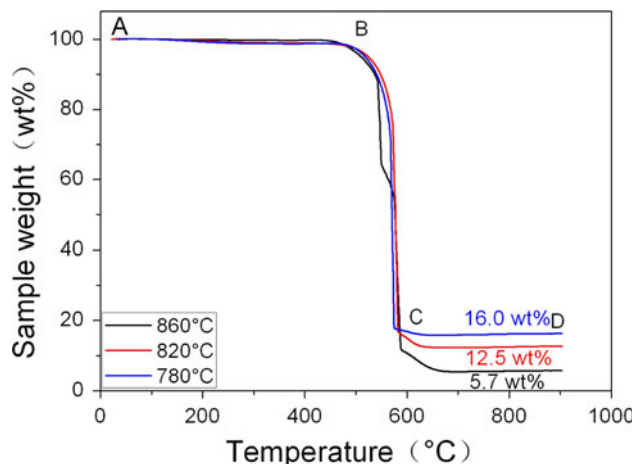


Fig. 3 Thermogravimetric analysis (TGA) of thin-walled open-ended aligned N-doped CNT samples produced at three different temperatures

keep constant and shows a platform in the TGA curve starting at about 650°C (see C → D part). N-doped CNTs turn into CO_2 or NO_x , and Fe metal was transformed into Fe_2O_3 when they are fully oxidized in air. Thus, we can obtain the Fe contents in products according to the weight

percentages of Fe_2O_3 residues after TGA measurements. It is found that the Fe content in the products grown at 780, 820, and 860°C are about 11.2, 8.6, and 3.9 wt%, respectively. It is also found that Fe encapsulation in CNTs decreased with temperature rising. A possible explanation is that more Fe was carried out of reaction zone by carrier gas with temperature rising.

In order to find out the distributions of diameter and TWI values, we measured 50 CNTs across a large sample area in each product by TEM observations. The statistical results of diameter values are shown in Fig. 4. The mean diameters of CNTs prepared at 780, 820, and 860°C are 35.5, 44.6, and 64.0 nm, respectively. Obviously, the diameters of CNTs increase as growth temperature rises from 780 to 860°C. The statistical results of TWI values are shown in Fig. 5. The mean TWI value of CNTs prepared at 780, 820, and 860°C is 2.8, 3.1, and 6.2, respectively. The CNTs prepared at 860°C have a larger TWI than that of CNTs prepared by using trichlorobenzene as carbon source ~5.0 [16]. Apparently, the TWI value has a similar temperature effect as that of diameters. This effect can in turn provide a convenient way to control the diameter and TWI of CNTs.

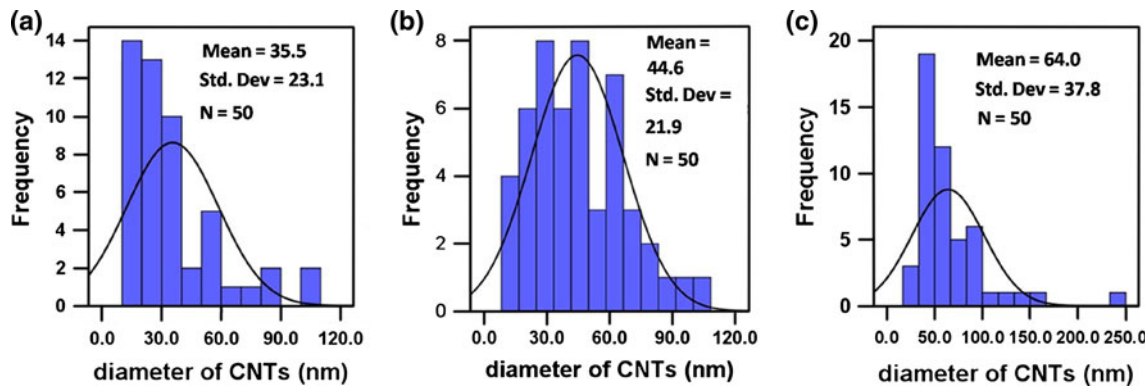


Fig. 4 The diameter distributions of the CNTs produced at different temperatures: **a** 780°C, **b** 820°C, **c** 860°C

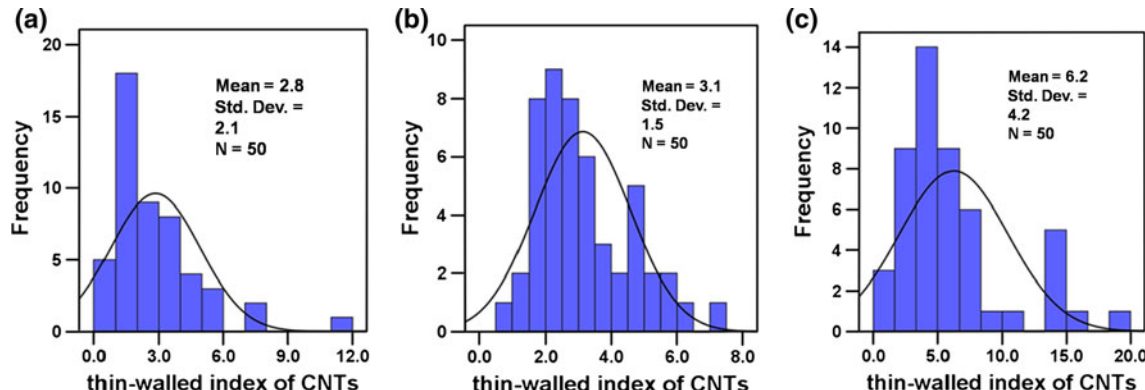
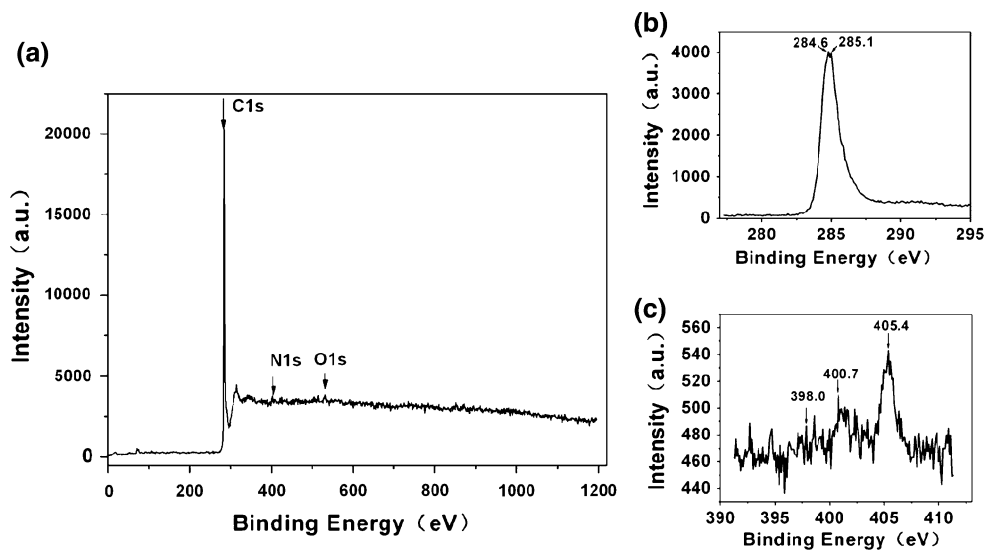


Fig. 5 The thin-walled index (TWI, defined as the ratio of inner diameter and wall thickness of a CNT) of the CNTs produced at different temperatures: **a** 780°C, **b** 820°C, **c** 860°C

Fig. 6 X-ray photoelectronic spectra of CNTs grown at 860°C: **a** the full spectrum, **b** C1s spectrum, **c** N1s spectrum



The XPS spectrum of the sample grown at 860°C is shown in Fig. 6. It can be seen that the product consists of C (96.57 at.%), O (1.86 at.%), N (1.21 at.%), and a small amount of Fe (0.18 at.%). It is obvious that the amount of iron is quite different between XPS and TGA analysis, because the former is surface analysis technique, while the latter is bulk analysis one. The presence of oxygen peak can be attributed to the prolonged exposure of the sample in the air atmosphere [31, 33]. The full spectrum, C1s spectrum and N1s spectrum are shown in Fig. 6a–c, respectively.

The Raman spectra of the CNTs grown at different temperatures are shown in Fig. 7. Raman spectroscopy has been shown to be a perfect tool to evaluate the crystallinity and the defects in carbon structures [30]. In Fig. 7, the strong band around $1,585\text{ cm}^{-1}$ is referred to the G-band,

Table 1 The I_D/I_G ratio of the CNTs produced at the three different temperatures

Temperature (°C)	780	820	860
I_D/I_G ratio	0.90	0.87	0.92

and the strong band around $1,335\text{ cm}^{-1}$ is referred to the D-band. The D-band corresponds to the defects and disordered in the graphene sheets, and the G-band is attributed to the well-graphitized carbon nanotubes [31]. The intensity ratio of D-band and G-band (I_D/I_G) were found to be ~ 1 for all the CNTs grown at the three different temperatures, as shown in Table 1. The large ratio of I_D/I_G is mainly attributed to the nitrogen doping into the CNTs. And the large I_D/I_G indicated that there were many defects in the CNTs, which could act as effective emission sites [14].

In order to evaluate the field-emission performance, CNT samples were also grown on silicon wafers. Figure 8 displays the typical morphology of the as-prepared CNTs, which grown homogeneously on silicon wafer or quartz slide (see Fig. 8a). It can be seen that CNTs grown on silicon wafer are well-aligned at all the three temperatures from SEM observations (see Fig. 8b–d). The field-emission measurements were carried out in a vacuum chamber of 2.2×10^{-6} Torr with CNT samples on silicon wafer as cathode.

Figure 9 shows the field-emission current (J) versus applied electric field (E) characteristics of thin-walled open-ended aligned N-doped CNTs grown at different temperatures. Here, the turn-on field (E_{to}) and threshold field (E_{th}) are defined as the electric fields when the emission current densities reach at $10\text{ }\mu\text{A}/\text{cm}^2$ and $1.0\text{ mA}/\text{cm}^2$, respectively [5]. Field-emission values of different samples are shown in Table 2. It can be seen that thin-walled open-ended aligned

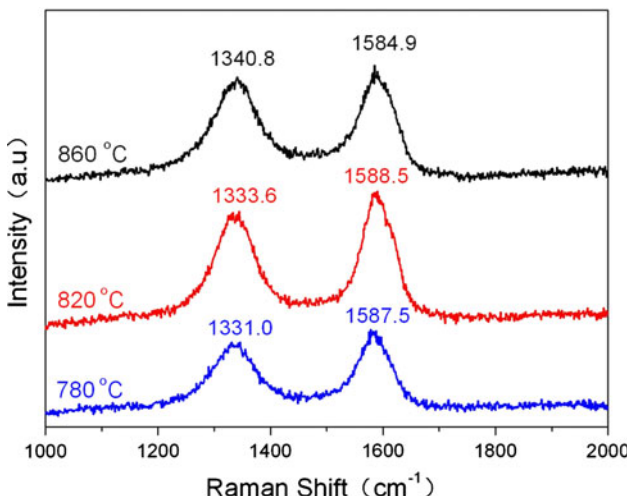


Fig. 7 Raman analysis of thin-walled open-ended aligned N-doped CNT samples produced at three different temperatures

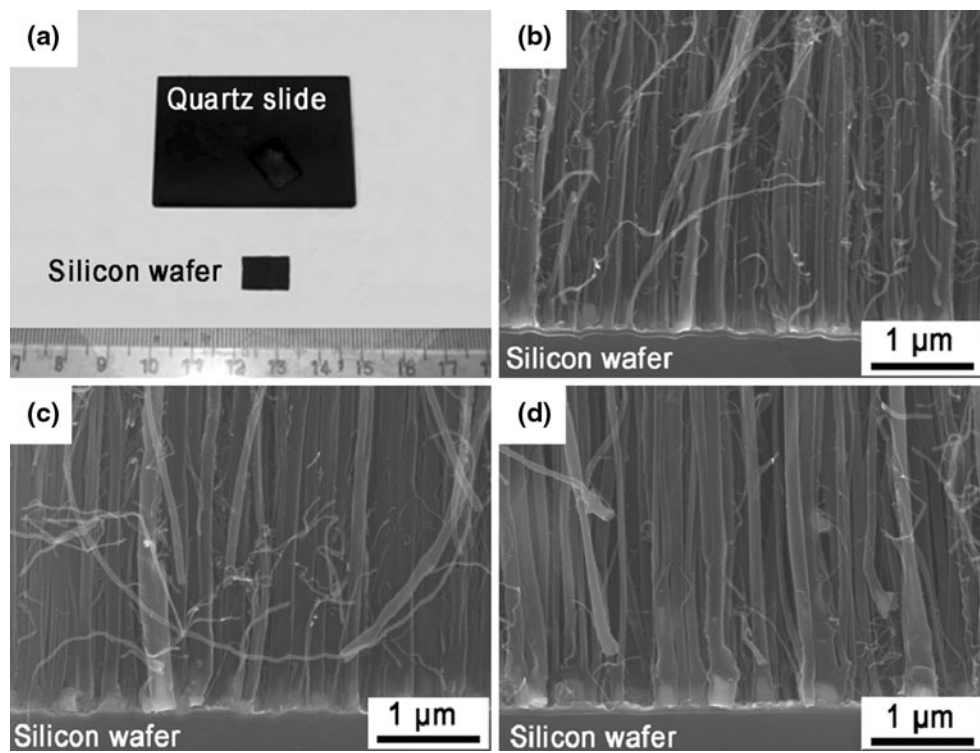


Fig. 8 Morphology of the as-grown products: **a** photograph of the products grown on silicon wafers and quartz slide, **b** SEM image of CNTs grown at 780°C on silicon wafer, **c** SEM image of CNTs grown at 820°C on silicon wafer, **d** SEM image of CNTs grown at 860°C on silicon wafer

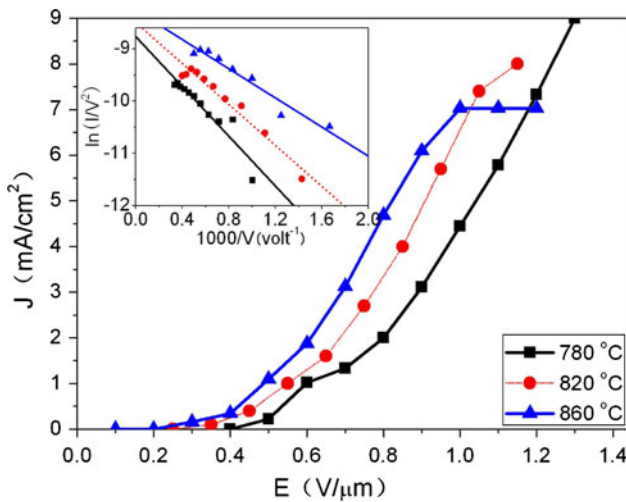


Fig. 9 Field-emission current (J) versus applied electric field (E) characteristics of thin-walled open-ended aligned N-doped CNTs grown at three different temperatures and the inset is the corresponding Fowler–Nordheim plots of different samples

N-doped CNTs show excellent field-emission properties. The CNTs prepared at 780, 820, 860°C show E_{to} of 0.45, 0.35, and 0.27 V/μm, respectively; and E_{th} of 0.60, 0.55, and 0.49 V/μm, respectively. This result illustrated that thinner sidewalls are favorable to the improvement of field-emission properties. From Table 2, one can see that

as-prepared thin-walled open-ended well-aligned N-doped CNTs show much lower turn-on field and threshold field than semiconductor nanomaterials (e.g., ZnO nanoneedle arrays [34], ZnS Tetrapod Tree-like Heterostructures [35], CuO nanoneedle arrays [36]), unfilled CNTs (e.g., Multi-walled CNTs grown on a graphitized carbon fabric [37], SWCNTs [38], aligned carbon nanotubes on plastic substrates [18]), N-doped CNTs (e.g., aligned N-doped CNTs [14], N-doped double-walled CNTs [39]), and FeNi-filled CNTs [5]. The inset of Fig. 9 is the corresponding Fowler–Nordheim (F–N) plots of different samples. The F–N plots show linear behavior, which is similar to many other reports [40, 41].

The field-enhancement factors (β) were calculated from the slopes of F–N plots (S_{F-N}) according to the following equation [5]:

$$\beta = B\varphi^{3/2}d/S_{F-N} \quad (1)$$

where φ is the work function of CNTs (=5.0 eV [5]), d is the emitting distance (=2.0 mm), and $B = 6.83 \times 10^9 \text{ V}/(\text{eV}^{3/2} \text{ m}^{-1})$ [5]. The field-enhancement factors were calculated and listed in Table 2, and the results showed that the field-enhancement factors had been significantly improved.

Free-standing membranes of thin-walled open-ended aligned N-doped CNTs were also prepared. As shown in

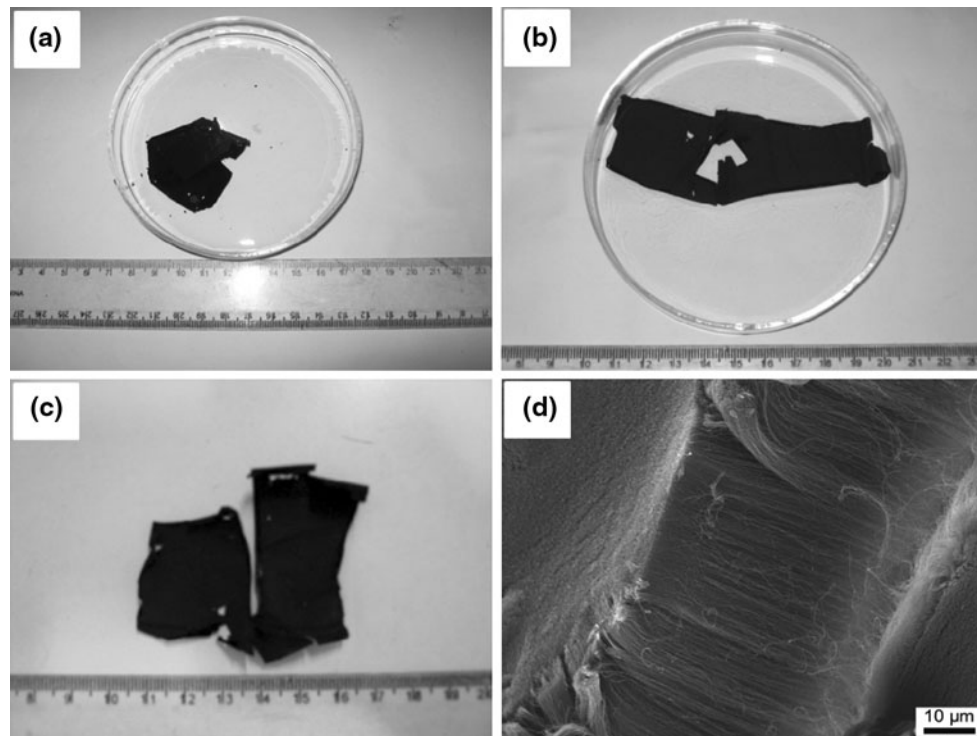
Table 2 Field-emission data of different samples, here E_{to} (V/ μm) and E_{th} (V/ μm) are turn-on electric field and threshold electric field, respectively; β is the field-enhancement factor

Samples	E_{to} (V/ μm)	E_{th} (V/ μm)	β	Data source
ZnO nanoneedle arrays	5.7	—	793	[34]
ZnS heterostructures	2.66	4.01	>2,600	[35]
Aligned N-doped CNTs	2.30	—	—	[14]
MWCNT	1.88	2.40	1.86×10^4	[37]
SWCNTs	—	2.40	3,392	[38]
Aligned CNTs	1.13	2.25	6,222	[18]
N-doped DWCNTs	~ 0.9	1.78	3,399	[39]
CuO nanoneedle arrays	0.85	—	—	[36]
FeNi-CNTs	0.30	0.65	2.48×10^4	[5]
ANCNT(780) ^a	0.45	0.60	6.41×10^4	This study
ANCNT(820) ^a	0.35	0.55	7.79×10^4	This study
ANCNT(860) ^a	0.27	0.49	1.09×10^5	This study

^a ANCNT (860), ANCNT (820), and ANCNT (780) denote the samples prepared by acetonitrile at a growth temperature of 860, 820, and 780°C, respectively

Fig. 8a, CNTs grow uniformly on quartz slide. Many practical applications of CNTs require the transfer of nanotube arrays onto other substrates [17]. Due to the Van der Waals forces in the vertically aligned nanotube arrays, the direct mechanical peeling of CNT membranes from the substrate will damage the alignment of nanotubes in the membranes [17]. It is still a challenge to obtain free-standing CNT membranes without destroying their

alignment. In this study, the quartz slide growing CNTs is put into 200 ml 10% HF solution for 12 h; then the CNT membranes can be peeled from the quartz slide directly, and then the CNT membranes was transferred into 100 ml water easily (see Fig. 10a). Next, 2–3 ml ethanol was added to the water, which made it easily for the flotation of CNT membranes to the water surface [42]. We also found that adding some ethanol to the water made it easier for the

**Fig. 10** CNT film peeled off and its SEM image: **a** CNT film peeled off from quartz slide and transferred into water, **b** CNT film spreading after dropping some ethanol to water, **c** the free-standing film obtained after drying in oven, **d** SEM image of the as-obtained CNTs

spreading of CNT membranes, as it could be seen in Fig. 10b. One can vividly see that as-obtained CNT membranes were about $30 \times 50 \text{ mm}^2$ as large as the size of the quartz slide (the quartz slide is $30 \times 50 \text{ mm}^2$ in dimension) from Fig. 10c. It is shown in Fig. 10d that the as-obtained CNTs are still well-aligned. The resulting free-standing film can be easily transferred onto other substrates (e.g., copper foil), which is a good news to their applications in different areas.

Conclusions

Thin-walled, open-ended, and well-aligned N-doped CNTs were synthesized by using acetonitrile as a carbon source. Temperature effects on diameter, TWI of as-produced CNTs and Fe encapsulation in the CNTs were also investigated. The resulting CNTs grown at 860°C exhibited much enhanced field-emission properties with a low turn-on field ($0.27 \text{ V}/\mu\text{m}$), threshold field ($0.49 \text{ V}/\mu\text{m}$), and high field-enhancement factor (1.09×10^5). A simple method is proposed to obtain free-standing membranes of this kind of CNTs. The free-standing membranes may find their applications in the supercapacitors, alkaline fuel cells, lithium ion batteries, and heat conductive material.

Acknowledgments The authors are grateful to the financial support from the National Natural Science Foundation of China (Grant No. 50902080, 50632040) and China Postdoctoral Science Foundation (Grant No. 20090450021).

Open Access This article is distributed under the terms of the Creative Commons Attribution Noncommercial License which permits any noncommercial use, distribution, and reproduction in any medium, provided the original author(s) and source are credited.

References

1. S. Iijima, Nature **354**, 56 (1991)
2. R.P. Raffaele, B.J. Landi, J.D. Harris, S.G. Bailey, A.F. Hepp, Mater. Sci. Eng. B **116**, 233 (2005)
3. Y. Chen, D.T. Shaw, L.P. Guo, Appl. Phys. Lett. **76**, 2469 (2000)
4. M. Chhowalla, C. Ducati, N.L. Rupesinghe, K.B.K. Teo, G.A.J. Amaratunga, Appl. Phys. Lett. **79**, 2079 (2001)
5. R.T. Lv, F.Y. Kang, D. Zhu, Y.Q. Zhu, X.C. Gui, J.Q. Wei, J.L. Gu, D.J. Li, K.L. Wang, D.H. Wu, Carbon **47**, 2709 (2009)
6. H. Murakami, M. Hirakawa, C. Tanaka, H. Yamakawa, Appl. Phys. Lett. **76**, 1776 (2000)
7. T.J. Vink, M. Gillies, J.C. Kriege, H.J.J. van de Laar, Appl. Phys. Lett. **83**, 3552 (2003)
8. M.S. Wang, L.M. Peng, J.Y. Wang, C.H. Jin, Q. Chen, J. Phys. Chem. B **110**, 9397 (2006)
9. C.C. Chiu, T.Y. Tsai, N.H. Tai, Nanotechnology **17**, 2840 (2006)
10. M. Glerup, J. Steinmetz, D. Samaille, O. Stéphan, S. Enouz, A. Loiseau, S. Roth, P. Bernier, Chem. Phys. Lett. **387**, 193 (2004)
11. L.B. Hu, D.S. Hecht, G. Gruner, Nanotechnology **20**, 465304 (2009)
12. M. Radosavljević, J. Appenzeller, Ph. Avouris, J. Knoch, Appl. Phys. Lett. **84**, 3693 (2004)
13. M. Terrones, P.M. Ajayan, F. Banhart, X. Blase, D.L. Carroll, J.C. Charlier, R. Czerw, B. Foley, N. Grobert, R. Kamalakaran, P. Kohler-Redlich, M. Rühle, T. Seeger, H. Terrones, Appl. Phys. A **74**, 355 (2002)
14. Y.H. Lai, H.B. Lian, K.Y. Lee, Diamond Relat. Mater. **18**, 544 (2009)
15. R.B. Sharma, D.J. Late, D.S. Joag, A. Govindaraj, C.N.R. Rao, Chem. Phys. Lett. **428**, 102 (2006)
16. R.T. Lv, F.Y. Kang, W.X. Wang, J.Q. Wei, J.L. Gu, K.L. Wang, D.H. Wu, Carbon **45**, 1433 (2007)
17. L.J. Ci, S.M. Manikoth, X.S. Li, R. Vajtai, P.M. Ajayan, Adv. Mater. **19**, 3300 (2007)
18. T.Y. Tsai, C.Y. Lee, N.H. Tai, W.H. Tuan, Appl. Phys. Lett. **95**, 013107 (2009)
19. H.W. Gu, T.M. Swager, Adv. Mater. **20**, 4433 (2008)
20. J.Y. Wang, Z. Jin, J. Cheng, Y. Li, J. Phys. Chem. C **113**, 8132 (2009)
21. J. Chen, Y. Liu, A.I. Minett, C. Lynam, J.Z. Wang, G.G. Wallace, Chem. Mater. **19**, 3595 (2007)
22. K. Mukai, K.J. Asaka, T. Sugino, K.J. Kiyohora, I. Takeuchi, N. Terasawa, D.N. Futaba, K.J. Hata, T. Fukushima, T. Adia, Adv. Mater. **21**, 1582 (2009)
23. N.T. Hong, J.H. Yim, K.H. Koh, S. Lee, P.N. Minh, P.H. Khoi, J. Vac. Sci. Technol. B **26**, 778 (2008)
24. A. Popp, O. Yilmazoglu, O. Kaldirim, J.J. Schneider, D. Pavlidis, Chem. Commun. **22**, 3205 (2009)
25. S.Y. Chew, S.H. Ng, J.Z. Wang, P. Novák, F. Krumeich, S.L. Chou, J. Chen, H.K. Liu, Carbon **47**, 2976 (2009)
26. J.M. Tang, M.E. Itkis, C. Wang, X. Wang, Y. Yan, R.C. Haddon, Micro Nano Lett. **1**, 62 (2006)
27. P.G. Whitten, A.A. Gestos, G.M. Spinks, K.J. Gilmore, G.G. Wallace, J. Biomed. Mater. Res. **82B**, 37 (2007)
28. R.T. Lv, S. Tsuge, X.C. Gui, K. Takai, F.Y. Kang, T. Enoki, J.Q. Wei, J.L. Gu, K.L. Wang, D.H. Wu, Carbon **47**, 1141 (2009)
29. G.W. Wu, A.Y. Cao, B.Q. Wei, C.L. Xu, J. Liang, D.H. Wu, J. Tsinghua Univ. (Sci. Technol.) **42**, 151 (2002)
30. R.M. Yadav, P.S. Dabal, T. Shripathi, R.S. Katiyar, O.N. Srivastava, Nanoscale Res. Lett. **4**, 197 (2009)
31. P. Ghosh, M. Subramanian, R.A. Afre, M. Zamri, T. Soga, T. Jimbo, V. Filip, M. Tanemura, Appl. Surf. Sci. **255**, 4611 (2009)
32. R.T. Lv, L. Zou, X.C. Gui, F.Y. Kang, Y.Q. Zhu, H.W. Zhu, J.Q. Wei, J.L. Gu, K.L. Wang, D.H. Wu, Chem. Commun. **17**, 2046 (2008)
33. Y.G. Lin, Y.K. Hsu, C.T. Wu, S.Y. Chen, K.H. Chen, L.C. Chen, Diamond Relat. Mater. **18**, 433 (2009)
34. J.S. Wang, C.S. Yang, P.I. Chen, C.F. Su, W.J. Chen, K.C. Chiu, W.C. Chou, Appl. Phys. A **97**, 553 (2009)
35. Z.G. Chen, J. Zou, G. Liu, X.D. Yao, F. Li, X.L. Yuan, T. Sekiguchi, G.Q. Lu, H.M. Cheng, Adv. Funct. Mater. **18**, 3063 (2008)
36. R.C. Wang, C.H. Li, Cryst. Growth Des. **9**, 2229 (2009)
37. R.B. Rakhi, K. Sethupathi, S. Ramaprabhu, Carbon **46**, 1656 (2008)
38. Y.K. Ko, J.X. Geng, S.G. Jang, S.M. Yang, T.W. Jeong, Y.W. Jin, J.M. Kim, H.T. Jung, Carbon **47**, 1555 (2009)
39. K.Y. Chun, H.S. Lee, C.J. Lee, Carbon **47**, 169 (2009)
40. K.B.K. Teo, M. Chhowalla, G.A.J. Amaralntuga, W.I. Milne, G. Pirio, P. Legagneux, F. Wyczisk, D. Pribat, D.G. Hasko, Appl. Phys. Lett. **80**, 2011 (2002)
41. Y.M. Wong, W.P. Kang, J.L. Davidson, B.K. Choi, W. Hofmeister, J.H. Huang, Diamond Relat. Mater. **14**, 2078 (2005)
42. J.Q. Wei, H.W. Zhu, Y.H. Li, B. Chen, Y. Jia, K.L. Wang, Z.C. Wang, W.J. Liu, J.B. Luo, M.X. Zheng, D.H. Wu, Y.Q. Zhu, B.Q. Wei, Adv. Mater. **18**, 1695 (2006)